Published in final edited form as:
J Autoimmun. 2014 September ; 53: 67–77. doi:10.1016/j.jaut.2014.02.011.

LONGITUDINALLY EXTENSIVE NMO SPINAL CORD PATHOLOGY PRODUCED BY PASSIVE TRANSFER OF NMO-IgG IN MICE LACKING COMPLEMENT INHIBITOR CD59

Hua Zhang and **A.S. Verkman**
Departments of Medicine and Physiology, University of California, San Francisco, CA

Abstract

Spinal cord pathology with inflammatory, demyelinating lesions spanning three or more vertebral segments is a characteristic feature of neuromyelitis optica (NMO). NMO pathogenesis is thought to involve binding of immunoglobulin G anti-aquaporin-4 autoantibodies (NMO-IgG) to astrocytes, causing complement-dependent cytotoxicity (CDC) and secondary inflammation, demyelination and neuron loss. We investigated the involvement of CD59, a glycophosphoinositol (GPI)-anchored membrane protein on astrocytes that inhibits formation of the terminal C5b-9 membrane attack complex. CD59 inhibition by a neutralizing monoclonal antibody greatly increased NMO-IgG-dependent CDC in murine astrocyte cultures and *ex vivo* spinal cord slice cultures. Greatly increased NMO pathology was also found in spinal cord slice cultures from CD59 knockout mice, and *in vivo* following intracerebral injection of NMO-IgG and human complement. Intrathecal injection (at L5-L6) of small amounts of NMO-IgG and human complement in CD59-deficient mice produced robust, longitudinally extensive white matter lesions in lumbar spinal cord. Pathology was most severe at day 2 after injection, showing loss of AQP4 and GFAP, C5b-9 deposition, microglial activation, granulocyte infiltration, and demyelination. Hind limb motor function was remarkably impaired as well. There was partial remyelination and recovery of motor function by day 5. Our results implicate CD59 as an important modulator of the immune response in NMO, and provide a novel animal model of NMO that closely recapitulates human NMO pathology. Upregulation of CD59 on astrocytes may have therapeutic benefit in NMO.

Keywords

NMO; aquaporin-4; astrocyte; complement-dependent cytotoxicity; demyelination

Address correspondence to: Alan S. Verkman, M.D., Ph.D., 1246 Health Sciences East Tower, University of California, San Francisco, CA 94143-0521, U.S.A.; Phone: (415) 476-8530; Fax: (415) 665-3847; Alan.Verkman@ucsf.edu; http:/www.ucsf.edu/verklab.

1. INTRODUCTION

Neuromyelitis optica (NMO) is an autoimmune inflammatory disease of the central nervous system that produces demyelinating lesions in spinal cord and optic nerve, and, to a lesser extent, in brain [1, 2]. Most NMO patients are seropositive for autoantibodies against aquaporin-4 (AQP4), a water-selective channel expressed in astrocytes throughout the central nervous system, as well as in epithelial cells in some peripheral organs including kidney and stomach [3]. Immunoglobulin G anti-AQP4 antibodies, called NMO-IgG (or AQP4-IgG), are pathogenic in NMO by a mechanism that involves binding to astrocyte AQP4, complement-dependent cytotoxicity (CDC), antibody-dependent cell-mediated cytotoxicity (ADCC), and inflammation with a prominent granulocyte and macrophage response, which leads to secondary oligodendrocyte injury, demyelination and neuronal injury [4-8].

Complement plays a central role in NMO pathogenesis. NMO lesions show prominent vasculocentric deposition of activated complement [9-13]. NMO-IgG and complement produce CDC in AQP4-expressing cell cultures, and characteristic NMO pathology in *ex vivo* spinal cord slice and optic nerve cultures [14]. Intracerebral injection or continuous infusion of NMO-IgG and complement in mice produces characteristic NMO pathology [15-17]. An open-label trial (NCT00904826) of a monoclonal antibody, eculizumab, which binds to C5 and inhibit its cleavage by C5 convertase, showed benefit in NMO, reducing the recurrence rate in NMO patients with severe disease [18].

Motivated by the central role of complement and CDC in NMO pathogenesis, we postulated that complement inhibitor proteins might modulate the immune response in NMO, and perhaps explain, in part, the marked NMO pathology seen in spinal cord and optic nerve compared with brain and peripheral AQP4-expressing tissues. The major membrane-associated complement regulatory proteins in humans include CD59, CD55 (alternative name DAF, decay acceleration factor), CD46 (alternative name MCP, membrane cofactor protein) and CD35 (type 1 complement receptor) [19]. CD59 is a phosphoinositol-linked glycoprotein that inhibits the terminal membrane attack complex consisting of complement proteins C5b through C9 [20]. CD55 prevents the formation of C3–C5 convertases and accelerates the degradation of these preformed enzymes. CD35 and CD46 act as cofactors that inactivate C3b and C4b through factor I [19]. As described in the discussion section, loss-of-function mutations in complement inhibitor proteins cause human diseases.

Here, we investigated the role of CD59 in NMO pathogenesis. CD59 is the major complement inhibitor protein in human astrocytes and glioma cell lines [19, 21-23]. In mice, there are two isoforms of CD59, CD59a and CD59b, with only CD59a in the CNS where it is expressed mainly in astrocytes but weakly in oligodendrocytes and neurons [24]. We studied the role of CD59 in NMO using primary astrocyte cultures, *ex vivo* spinal cord slice cultures, and *in vivo* mouse models of NMO, including a novel intrathecal injection model. CD59 function was investigated using a specific neutralizing monoclonal antibody and CD59 knockout mice. We found remarkably increased NMO-IgG-dependent cytotoxicity and NMO pathology in CD59 knockout mice, with the development of longitudinally

extensive NMO pathology, as found in human NMO. The data implicate CD59 as an important determinant in NMO pathogenesis and hence a novel therapeutic target in NMO.

2. MATERIALS AND METHODS

2.1. Mice

In vivo studies were performed on 8-to-10-week-old, weight-matched BALB/c wild-type and $CD59^{-/-}$ mice ($CD59a^{tm1Song/tm1Song}$, purchased from MMRRC, Davis, CA) [25]. For behavioral testing, litter-matched wild-type and $CD59^{-/-}$ knockout mice were compared. Mice were maintained in air-filtered cages and fed normal mouse chow in the University of California, San Francisco (UCSF) Animal Care facility. All procedures were approved by the UCSF Committee on Animal Research.

2.2. Cell culture

Primary astrocyte cultures were prepared from cortex of wild-type and $CD59^{-/-}$ neonatal mice, as described [26]. Briefly, the cerebral hemispheres were isolated and cortical tissue was minced and incubated for 15 min at 37 °C in 0.25% trypsin-EDTA. Dissociated cells were centrifuged at 500 g for 5 min and resuspended in Dulbecco's Modified Eagle Medium (DMEM) containing 10% FBS and 1% penicillin/streptomycin in T75 flasks and grown at 37 °C in a 5% CO_2 incubator. After cell confluence (8-10 days), flasks were shaken in a rotator at 180 rpm overnight to purify astrocytes. The medium was replaced with DMEM containing 3% FBS and 0.25 mM dibutyryl cAMP (Sigma-Aldrich, St. Louis, MO) to induce differentiation. Cultures were maintained for up to an additional 2 weeks with twice weekly media changes. Immunocytochemistry showed that >95% of the cells stained for the astrocytic marker, glial fibrillary acidic protein (GFAP, Millipore, Billerica, MA).

2.3. Antibodies and sera

Recombinant monoclonal NMO antibody rAb-53 (referred to as NMO-IgG) was generated from a clonally expanded plasma blast population from cerebrospinal fluid of an NMO patient, as described and characterized previously [27, 28]. Briefly, antibody variable heavy and light chains were PCR-amplified from CD138+ plasma cells; one such recombinant antibody with high-affinity AQP4 binding, rAb-53, was generated using an IgG1 constant region. rAb-53 has been showed to produce NMO pathology *in vivo* and *in vitro* [7, 17, 28]. NMO serum was obtained from seropositive individuals who met the revised diagnostic criteria for clinical disease. Non-NMO (seronegative) human serum was used as control. In some studies IgG was purified from NMO or control serum using a Protein A-resin (GenScript, Piscataway, NY) and concentrated using Amicon Ultra Centrifugal Filter Units (Millipore).

2.4. Complement-dependent cytotoxicity (CDC)

Astrocyte cultures were trypsinized and re-plated onto 96-well microplates at a density of 20,000 cell/well and grown for 48 h. In some studies a CD59 neutralizing antibody (7A6, binding to CD59a, 10 μg/mL, provided by Dr. B.P. Morgan, Cardiff University, UK) or phosphatidylinositol-specific phospholipase C (PI-PLC, 0.5 U/mL, Invitrogen, Carlsbad, CA) were added 1 h prior to experiments. Human complement (Innovative Research, Novi,

MI) and NMO-IgG were then added in Hank's buffer, and cells were incubated at 28 °C for 2 h. Cytotoxicity was measured by the Alamar Blue assay (Invitrogen).

2.5. NMO-IgG binding

Astrocyte cultures were trypsinized and re-plated onto 96-well microplates at low density and grown for 48 h. As described [29], cells were incubated for 30 min in live cell blocking buffer (phosphate-buffered saline (PBS) containing 6 mM glucose, 1 mM sodium pyruvate, 1 % BSA) and then incubated for 2 h with NMO-IgG in blocking buffer. Cells were then rinsed in PBS, fixed in 4 % paraformaldehyde for 15 min, and permeabilized with 0.1 % Triton X-100. Cells were incubated for 60 min with 0.4 g/ml of a polyclonal, C-terminal-specific rabbit anti-AQP4 antibody (Santa Cruz Biotechnology, Santa Cruz, CA) and then for 30 min with 4 g/ml goat anti-human IgG-conjugated Alexa Fluor 488 and 4 g/ml goat anti-rabbit IgG-conjugated Alexa Fluor 555 (Invitrogen) in blocking buffer. Red and green fluorescence was imaged on a Nikon Eclipse TE2000S inverted epifluorescence microscope (Nikon, Melville, NY). Binding affinity was determined by nonlinear regression of background-subtracted green/red fluorescence intensity ratios [29].

2.6. In vivo intracerebral injection model

As described [17], mice were implanted with an osmotic minipump (Alzet 1003D, Cupertino, CA) with the needle positioned in the right lateral brain (from the bregma, medial-lateral +1.5 mm and dorsal-ventral +0.5 mm, 2.5 mm below the dura). NMO-IgG and human complement were dissolved in PBS and delivered for 3 days at 0.5 μg per day and 16.7 μl of per day, respectively. Control mice were implanted identically with an osmotic minipump that delivered control IgG and complement. Mice were perfused through the cardiac ventricle with 4% paraformaldehyde in saline and frozen sections of brain were cut at 10-μm thickness.

2.7. Ex vivo spinal cord slice model of NMO

Transverse slices of cervical spinal cord from 7-day old wild-type and $CD59^{-/-}$ mice were cut at 300-μm thickness using a vibratome (S1000, Leica, Wetzlar, Germany) and placed in ice-cold Hank's balanced salt solution (HBSS, pH 7.2), as described [14]. Slices were placed on transparent membrane inserts (Millipore, Millicell-CM 0.4-μm pores, 30 mm diameter) in 6-well plates containing 1 ml culture medium, with a thin film of culture medium covering the slices. Slices were cultured in 5 % CO_2 at 37 °C for 7 days in 50 % MEM, 25 % HBSS, 25 % horse serum, 1 % penicillin-streptomycin, 0.65 % glucose and 25 mM HEPES. Slices were then incubated with rAb-53 (10 μg/mL) and human complement (5 %), with or without the CD59a neutralizing antibody (7A6, 10 μg/mL) or PI-PLC (0.5 U/mL).

2.8. L5-L6 spinal cord intrathecal injection model

For intrathecal injection, mice were anesthetized using isoflurane. The spinal cord was punctured between L5 and L6 vertebra using a 28-gauge insulin needle to break the dura, which produced a tail flick indicating needle contact with nerve bundles at L6 [30]. A 30-gauge flat needle attached to 10 μl gas-tight glass syringe (Hamilton, Reno, NV) was inserted at the same position to infuse 10 μg of recombinant NMO-IgG or control IgG and 5

μL human complement in a total volume of 10 μl (at 10 μl/min). In some experiments 50 μg of IgG purified from NMO (or non-NMO) patient serum and 5 μL of human complement in a total volume of 10 μl was injected. In some experiments, Evans blue was injected to study diffusion. Mice were perfused with 4% paraformaldehyde in saline and frozen sections of spinal cord were cut transversely or longitudinally at 10-μm thickness.

2.9. Motor function behavioral analysis

Established ledge and hind limb clasping tests were used to score motor function. In the ledge test, mice were placed on the ledge of the cage, as described [31]. A wild-type mouse will typically walk along the ledge without losing balance, and lower itself back into the cage gracefully using its paws (scored as 0). Degrees of impairment include loss of footing while walking along the ledge, but otherwise good coordination (score 1), ineffective use of hind legs and landing on its head rather than its paws when descending into the cage (score 2), and falling from ledge while walking or attempting to lower itself, or shaking and refusing to move despite encouragement (score 3). Hind limb clasping has been used as a marker of disease progression in mouse models of neurodegeneration caused by demyelination and axon pathology [32]. The mouse is grasped by the tail near its base and lifted for 10 seconds. The hind limbs are consistently splayed outward away from the abdomen in a normal mouse (scored 0). Degrees of impairment include retractions of one hind limb toward the abdomen for >50% of the time suspended (score 1), partial retraction of both hind limbs toward the abdomen for >50% of the time suspended (score 2), and entire retraction of its hind limbs for >50% of the time suspended (score 3). The scores from the ledge and hind limb tests were summed and averaged. The assessments were performed blinded to mouse genotype and treatment condition. Each test was repeated 3 times. Some mice were subjected to footprint analysis [33] in which the hind limbs were covered by ink and the mouse was allowed to walk across a narrow strip of paper. Stride length was reported as the mean of 4-5 sequential steps.

2.10. Immunofluorescence

Cultured astrocytes and spinal cord slice cultures were fixed with 4% paraformaldehyde for 15 min and incubated in blocking solution (PBS containing 1% BSA and 0.2% Triton X-100) for 1 h. Frozen sections of brain and spinal cord were post-fixed with 4% paraformaldehyde for 5 min and incubated in blocking solution for 1 h. Slides were then incubated for 2 h with antibodies against GFAP (1:1000; Millipore), AQP4 (1:200, Santa Cruz Biotechnology), ionized calcium binding adaptor molecule 1 (Iba1; 1:1000, Wako, Richmond, VA), C9neo (1:100, Santa Cruz Biotechnology), myelin basic protein (MBP, 1:100, Santa Cruz Biotechnology), CD45 (1:10; BD Biosciences, San Jose, CA), anti-neutrophil (Ly6G antibody; 1:100; eBioscience, San Diego, CA), anti-eosinophil (Siglec F antibody; 1:50; BD Biosciences), albumin (1:100, Santa Cruz Biotechnology), cleaved Caspase-3 (Asp175) antibody (1:100, Cell Signaling, Danvers, MA), CD59 (7A6, 5 μg/mL), CD55 (clone RIKO-3, LifeSpan BioSciences, Seattle, WA), βIII tubulin (Tuj1, 1:500, Millipore) and Olig2 (1:200, Millipore), followed by the appropriate species-specific Alexa Fluor–conjugated secondary antibody for 1 h (5 g/ml each, Invitrogen). In some experiment, CD59 (7A6) antibody was biotinylated (Miltenyi Biotec Inc, Auburn, CA) and detected by streptavidin-Alexa Fluor® 555 Conjugate (Invitrogen) to reduce background. After rinsing

in PBS, sections were mounted with VectaShield (Vector Laboratories, Burlingame, CA). Immunofluorescence was visualized on a Leica fluorescence microscope or Nikon confocal microscope.

2.11. Immunoblot

Mice tissues were isolated and homogenized in RIPA buffer (Cell Signaling) containing serine protease inhibitor (Sigma). Homogenates were centrifuged at 1500 g for 5 min and the supernatant was collected and stored at −80 °C. Protein concentration was measured using the Bio-Rad Protein Assay Kit II (Bio-Rad Laboratories, Hercules, CA). Proteins were resolved on 12% BT SDS-PAGE gels (Invitrogen) and electrotransferred to a nitrocellulose membrane. The membrane was incubated with rabbit anti-AQP4 or rabbit anti-CD59 antibody (Santa Cruz Biotechnology) or anti-β-actin antibody (GE Healthcare, Piscataway, NJ) followed by horseradish peroxidase-linked anti-rabbit IgG or anti-mouse IgG (1:10.000, GE Healthcare), and visualized by enhanced chemiluminescence (GE Healthcare).

3. RESULTS

3.1. CD59 expression in mouse central nervous system and peripheral tissues

Immunofluorescence showed CD59 expression throughout mouse brain, spinal cord and optic nerve, with more in white than gray matter in brain and spinal cord (Fig. 1a). Spinal cord sections showed partial CD59 co-localization with astrocyte marker AQP4 and oligodendrocyte marker MBP in white matter (Fig. 1b); high magnification showed CD59 expression on astrocytes and oligodendrocytes in white matter (Fig. 1c). In spinal cord grey matter, CD59 is coexpressed with AQP4 at relatively low density, with little CD59 on astrocyte end-feet where AQP4 is enriched; CD59 was not seen on neurons or microglia (Fig. 1c). In kidney, CD59 was seen in multiple cell types with enrichment in collecting duct epithelial cells where AQP4 is expressed (Fig. 1d). CD59 was also expressed strongly in skeletal muscle, where AQP4 is weakly expressed. Immunoblot analysis of tissue homogenates showed high AQP4 expression throughout the CNS, greater in homogenates of spinal cord and optic nerve than brain, with relatively little AQP4 in kidney and skeletal muscle homogenates (Fig. 1e). Though AQP4 expression is high in kidney collecting duct cells as seen in Fig. 1d, the collecting duct makes up only a small part of total kidney homogenate, which is the reason for the lack of detection by immunoblot. CD59 expression was low in homogenates of spinal cord, hippocampus and optic nerve, and relatively high in kidney and skeletal muscle.

3.2. CD59 protects astrocytes from NMO-IgG and complement-dependent cytotoxicity

AQP4 and CD59 were strongly expressed at the plasma membrane in well-differentiated primary astrocyte cultures from wild-type ($CD59^{+/+}$) mice (Fig. 2a). CD59 immunofluorescence was not seen in astrocytes from $CD59^{-/-}$ mice. The $CD59^{+/+}$ and $CD59^{-/-}$ astrocytes showed no CD55 expression. AQP4 expression and binding of NMO-IgG to AQP4 were comparable in the $CD59^{+/+}$ and $CD59^{-/-}$ astrocyte cultures (Fig. 2b).

The $CD59^{-/-}$ astrocyte cultures were remarkably more susceptible to CDC than the $CD59^{+/+}$ cultures, as measured using an Alamar blue assay following incubation with NMO-IgG and

human complement (Fig. 2c). Increased susceptibility was also seen following treatment of $CD59^{+/+}$ astrocyte cultures with a CD59 neutralizing antibody [34], or with PI-PLC, which cleaves all membrane-bound GPI proteins including CD59 and CD55 (Fig. 2d) [35, 36]. PI-PLC treatment did not further increase CDC in the $CD59^{-/-}$ astrocyte cultures (Fig. 2d), supporting the conclusion that CD59 is the major complement inhibitor protein on mouse astrocytes.

3.3. CD59 protects against NMO pathology in ex vivo spinal cord slice cultures

CD59 function was also studied in an *ex vivo* spinal cord slice culture model in which NMOIgG and complement exposure produces loss of AQP4, GFAP and myelin [14]. Vibratome-cut spinal cord slices from 7-day-old $CD59^{+/+}$ and $CD59^{-/-}$ mice were cultured for 7 days, then submaximal NMOIgG and human complement were added for 24 h, after which slices were immunostained for markers of NMO pathology. Fig. 3a shows AQP4, GFAP and MBP immunofluorescence, together with lesion scores (0: no pathology; 4: severe pathology). Marked loss of AQP4 and GFAP was seen in the $CD59^{-/-}$ slices, with little pathology in the $CD59^{+/+}$ slices under the conditions of the experiment. Treatment of $CD59^{+/+}$ slice cultures with the mCD59a neutralizing antibody or with PI-PLC greatly increased NMO-IgG and complement-dependent pathology.

As CD59 prevents membrane attack complex formation, we confirmed increased C9neo deposition on the $CD59^{-/-}$ spinal cord slice cultures. In $CD59^{+/+}$ slice cultures C9neo deposition was seen at 6 h with little at 2.5 h, whereas in the $CD59^{-/-}$ slice cultures C9neo deposition was seen at 2.5 h, and was quite marked at 6 h (Fig. 3b). Greater C9neo deposition was also seen in the $CD59^{+/+}$ slice cultures treated with CD59 neutralizing antibody or PI-PLC. PI-PLC did not further increase C9neo deposition in the $CD59^{-/-}$ slice cultures. At 6 h there was little effect on AQP4 staining in both the $CD59^{+/+}$ and $CD59^{-/-}$ slice cultures (not shown), whereas AQP4 staining was reduced at 24 h as seen in Fig. 3a.

3.4. CD59 deficiency increases NMO pathology in brain produced by intracerebral infusion of NMO-IgG and complement

We postulated that the increased susceptibility of CD59-deficient astrocyte cultures to CDC, and of spinal cord slice cultures to NMO pathology, would translate to increased NMO susceptibility *in vivo*. In a first set of studies submaximal NMO-IgG and human complement was infused continuously into mouse brain over 3 days (Fig. 4a). Under these conditions small lesions with loss of AQP4 and MBP were seen in brains of $CD59^{+/+}$ mice, which were much larger in brains of $CD59^{-/-}$ mice (Fig. 4b). In control studies infusion of complement and control-IgG did not produce NMO pathology in the $CD59^{+/+}$ or $CD59^{-/-}$ mice. Staining with an anti-human secondary antibody (Fig. 4a, top row of micrographs) showed comparable areas of NMO-IgG deposition in this model. $CD59^{-/-}$ mice showed areas of parallel AQP4 and MBP loss, whereas $CD59^{+/+}$ mice showed less loss of MBP than AQP4 (Fig. 4c, d). Greater inflammation was seen in the $CD59^{-/-}$ mice, as judged from CD45-positive leukocytes and Iba1-positive microglia/macrophages in the lesion (Fig. 4c).

3.5. Intrathecal administration of NMO-IgG and complement produces longitudinally extensive white-matter lesions in CD59-deficient mice

A major pathological feature in spinal cord in human NMO is demyelinating pathology spanning three or more vertebral segments. NMO-IgG and human complement were injected intrathecally between L5 and L6 levels (Fig. 5a, left). As shown by the Evans blue diffusion (Fig. 5a, middle), the injected dye diffused to the lumbar spinal cord subarachnoid space by 1 hour and throughout the cerebral ventricles by 24 hours. Notably, lesions were seem mainly in the lumbar spinal cord and not in brain, which might due to limited diffusion limit of NMO-IgG and/or human complement. Fig. 5a (right) shows longitudinally extensive spinal cord pathology (over 3 segments) in a $CD59^{-/-}$ mouse at 2 days after NMO-IgG and complement injection, as seen by loss of AQP4 near the pia matter and at multiple locations in white matter. $CD59^{+/+}$ mice showed no pathology with the same amount of injected NMO-IgG and human complement, indicating a major protective role of CD59 in this model. High magnification immunofluorescence of human IgG and AQP4 in Fig. 5b shows greater antibody deposition and AQP4 loss in spinal cord slices from $CD59^{-/-}$ than $CD59^{+/+}$ mice. Administration of NMO-IgG or human complement individually did not cause pathology in $CD59^{-/-}$ mice or $CD59^{+/+}$ mice. Longitudinally extensive loss of AQP4 and GFAP in white matter, as well as albumin extravasation, was seen in $CD59^{-/-}$ mice (Fig. 5c), indicating blood-spinal cord barrier disruption. Transverse sections also showed extensive damage to pia matter and much of the white matter, with loss of AQP4 and GFAP in the lesions, and reactive astrocytes with increased GFAP staining near the lesions (Fig. 5c). High magnification (right panels in Fig. 5c) showed reduced MBP in $CD59^{-/-}$ mice with destruction of the normal nerve pattern near the dorsal horn. The pathology in spinal cord white matter lesions is similar to that reported in human NMO lesions [12, 14, 37]. $CD59^{-/-}$ mice showed loss of AQP4, GFAP and MBP, motor neuron apoptosis (cleaved caspase 3), deposition of NMO-IgG and C9neo, and infiltration of macrophages/microglia, neutrophils and eosinophils in the spinal cord white matter (Fig. 5d). Fig. 5e indicates significantly reduced MBP and AQP4 in the L5 segment of spinal cord white matter in the $CD59^{-/-}$ mice at day 2.

Behavioral studies showed impaired motor function in the $CD59^{-/-}$ mice receiving intrathecal NMO-IgG and complement. At day 2, gait abnormalities were seen as assessed from footprint pattern analysis during ambulation along a narrow corridor (Fig. 6a). Control mice ambulated in a straight line with a regular alternating gait, whereas the $CD59^{-/-}$ mice receiving NMO-IgG and complement showed shorter average stride length. $CD59^{+/+}$ mice receiving NMO-IgG and complement showed no difference in stride length. The ledge test, which assesses hind limb weakness, showed progressive impairment in motor function beginning by day 2, with partial recovery at day 5 (Fig. 6b). Only minor motor impairment was seen in identically treated $CD59^{+/+}$ mice and in $CD59^{-/-}$ mice treated with control IgG. Similar studies done in $CD59^{-/-}$ mice administered purified IgG from human NMO sera together with complement also showed impairment in motor function (Fig. 6c).

To characterize the time course over which NMO pathology develops, $CD59^{-/-}$ and $CD59^{+/+}$ mice receiving NMO-IgG or control antibody were sacrificed at 1 and 5 days after intrathecal administration of NMO-IgG and complement. Fig. 6d shows early astrocyte

damage at day 1 with loss of AQP4 and abnormal GFAP morphology in white matter. Marked inflammation was seen as infiltration of neutrophils and macrophages/microglia; however, myelin was preserved at 1 day. Partial recovery was seen at day 5 with increased AQP4 and GFAP expression (Fig. 6e, top). Loss of myelin and aggregated microglia/macrophage were seen in the lesions, with few neutrophils and eosinophils (data not shown). Interestingly, more grey matter lesions were seen at day 5, with loss of AQP4 and an abnormal pattern of GFAP expression near blood vessels (Fig. 6e, bottom). Microglia near the lesion were activated, but no loss of MBP was seen. Fig. 6f shows early AQP4 loss at day 1 in spinal cord white matter, which was greater at day 2, with partial recovery at day 5. Reduced MBP was seen at days 2 and 5. At day 5, remyelination was seen as increased number of Olig 2-positive oligodendrocyte precursor cells in white matter where the myelin was lost (Fig. 6g).

3.6. Increased CD59 expression in wild-type mice following NMO-IgG and complement administration

We investigated the possibility that CD59 up-regulation might occur following induction of spinal cord NMO pathology, which may be a compensatory protective response. Fig. 7a shows a robust increase in CD59 immunofluorescence in white matter of lumbar spinal cord in $CD59^{+/+}$ mice. Immunoblot also showed increased CD59 in lumbar spinal cord of mice receiving NMO-IgG and complement but not in control mice receiving NMO-IgG only or complement together with control IgG (Fig. 7b). In the brain infusion model, up-regulation of CD59 was seen near lesions, both on oligodendrocytes and astrocytes (Fig. 7c).

4. DISCUSSION

The major findings of this study are: *(i)* greatly increased cytotoxicity and NMO pathology produced by NMO-IgG and complement following CD59 inactivation; *(ii)* development of longitudinally extensive NMO pathology in CD59-deficient mice following a single intrathecal injection of NMO-IgG and complement; and *(iii)* up-regulation of CD59 around NMO lesions. CD59 is a 77-amino acid membrane glycoprotein that regulates the terminal components of the complement pathway by inhibiting formation of the cytolytic membrane attack complex. The membrane attack complex, which is formed by the assembly of C5b, C6, C7, C8 and multiple C9 molecules, is inhibited by CD59 [20]. We found here that functional inactivation of CD59 by a neutralizing antibody or by the enzyme PI-PLC greatly increased astrocyte susceptibility to CDC, as did CD59 deletion in mice, which translated to more severe NMO pathology following passive transfer of NMO-IgG in mice and development of human-like spinal cord pathology. In mice, there are two CD59 isoforms – CD59a and CD59b. CD59a in mice resembles human CD59 as it is broadly distributed and functions to regulate assembly of the membrane attack complex. CD59b, encodes a CD59-like protein expressed only in testis [38]. Our study here applies to mouse CD59a, as CD59a deficient mice and CD59a neutralizing antibody were used.

Complement can be activated by 3 pathways – the classical, alternative, and lectin pathways [19, 39]. Complement dysregulation can produce inappropriate overactivation and autoimmune disease [39]. The classical complement pathway is of primary importance in

NMO [1]. Mutations affecting complement regulators, including factor H, factor I, factor B and CD46, are associated with atypical hemolytic-uremic syndrome, membranoproliferative glomerulonephritis, dense-deposit disease, C3 glomerulonephritis and the HELLP syndrome of pregnancy [40].

CD59 deficiency in humans causes paroxysmal nocturnal hemoglobinuria in which chronic hemolysis results from hypersensitivity of erythrocytes to complement-mediated lysis. CD59 deficiency in this disease can result from mutation in the PIGA (phosphatidylinositol N-acetylglucosaminyltransferase subunit A) gene on the X chromosome, which impairs GPI anchor function and CD59 cell surface expression [41]. A point mutation in CD59 was also reported as the etiology of chronic hemolysis and childhood relapsing immune-mediated polyneuropathy [42]. With regard to CNS-related diseases, $CD59^{-/-}$ mice show worse outcome in models of Alzheimer's disease, brain traumatic injury, focal cerebral ischemia and experimental allergic encephalomyelitis [24, 43-46]. CD59 deficiency has not been reported in NMO. Our study suggests that astrocyte CD59 is protective against NMO-IgG induced pathology. The relatively high expression of CD59 in optic nerve and spinal cord white matter may play a protective role in NMO. We speculate that down-regulation of CD59 expression might trigger NMO disease. CD59 expression is altered in some bacterial and viral infections, including hepatitis B [47] and the bacterial toxin intermedilysin [48]; several papers speculate without direct evidence that bacterial or viral infections are risk factors in NMO [49]. Hyper-glycation of K41 in CD59 in type I diabetes produces loss of function [42, 50]. Several case reports describe the co-existence of the other autoimmune disorders with NMO, including insulin-dependent diabetes mellitus [51] and diabetes-related peripheral neuropathy [52].

CD59 expression is relatively low in whole brain, as found here and in prior studies [38, 53]. However, CD59 is highly expressed on human peripheral blood leukocytes and erythrocytes, as well as on endothelial cells, Schwann cells and some epithelial cells including salivary gland acinar cells, bronchial epithelium, renal tubules and brain ependymal cells [38]. CD59 may thus play a protection role prevent NMO pathology in peripheral, AQP4-expressing tissue. In addition to CD59, the major membrane-associated complement regulatory proteins in humans include CD55, CD46 and CD35. CD55 and CD46 are relatively low in brain [54]; CD35 is absent in neurons and astrocytes [53]. CD55 was not detectable in mouse astrocyte in our study here, and we did not study CD35 or CD46.

Modulation of complement inhibitor protein expression or activity has potential therapeutic utility. The reported benefit of eculizumab in a small, open-label clinical trial supports the utility of complement inhibition in NMO [18], as does our recent report demonstrating the potential utility of a C1q-neutralizing monoclonal antibody [55]. The data here suggest increased CD59 activity may reduce CDC and downstream inflammatory demyelination in NMO. However, whether pharmacological up-regulation of CD59 would be beneficial is unclear based on the mouse data here showing up-regulation of CD59 following induction of NMO pathology. It was reported that cytokines, including TNF-α, IL-1β and IL-6, cause up-regulation of CD55 and CD59 in human hepatoma cells [56] and human vascular endothelial cells [57], suggesting that the up-regulation of CD59 found here might be caused by increased cytokines in NMO lesions. In some tumor cell lines, sublytic membrane attack

complex activation was reported to cause CD59 up-regulation by calcium-dependent PKA and ERK signaling pathways [58, 59]. A soluble form of CD59, sCD59, has been shown to have benefit in models of macular degeneration [60] and hepatic vascular endothelial disease [61]. sCD59 fusions with membrane-binding peptide or Fc fusions protein have shown benefit in a rat model of rheumatoid arthritis and a mouse model of AMD [62, 63].

Intrathecal injection is widely used in rat models in the pain field to locally administer various agents to the L4-L6 spinal cord [64], but this approach has been used less frequently in mice because of its technical difficulty and limitations in injected volume. The first application, reported in the 1980s, was of intrathecal injection of morphine in mice [30]. We adapted the method by injecting small amounts of human complement and NMO-IgG between the L5 and L6 intervertebral space, with a greater than success in >80% of mice. Injection of the same volume (10 μL) of vehicle did not produce pathology or motor deficit. The diffusion of injected dye was slow due to the small cerebrospinal fluid space in spinal cord, but after 24 h dye diffused into brain ventricles. The NMO pathology here was found primarily in the lumbar area, which is probably related to the relatively high concentration of complement. Though little NMO pathology was seen in wild-type mice, robust, longitudinally extensive pathology was produced in $CD59^{-/-}$ mice following intrathecal administration of NMO-IgG and complement. This model thus provides a potentially useful animal model of NMO spinal cord disease. Prior models in which spinal cord pathology is seen involve NMO-IgG administration to rats with pre-existing neuroinflammation produced by EAE [27, 65]. In mice, intrathecal injection of complement and NMO-IgG from the cisterna magna in wild-type mice produced minor ependymal damage after 7 days but no spinal cord pathology [66].

In conclusion, our results implicate CD59 as an important determinant in NMO pathogenesis, as it is a major regulator of NMO-IgG and complement-dependent cytotoxicity in astrocytes, the initiating pathogenic process leading to inflammation, oligodendrocyte injury and demyelination. CD59 up-regulation thus provides a novel and potentially efficacious approach to reduce NMO pathology.

Acknowledgments

This work was supported by grants EY13574, EB00415, DK35124, and DK72517 from the National Institutes of Health, and a grant from the Guthy-Jackson Charitable Foundation. We thank Dr. Jeffrey Bennett (Univ. Colorado Denver, Aurora, CO) for providing recombinant monoclonal NMO antibody and for Accelerated Cure (Waltham, MA) for providing human NMO sera.

REFERENCES

[1]. Jarius S, Paul F, Franciotta D, Waters P, Zipp F, Hohlfeld R, et al. Mechanisms of disease: aquaporin-4 antibodies in neuromyelitis optica. Nat Clin Pract Neurol. 2008; 4:202–14. [PubMed: 18334978]

[2]. Wingerchuk DM, Lennon VA, Lucchinetti CF, Pittock SJ, Weinshenker BG. The spectrum of neuromyelitis optica. Lancet Neurol. 2007; 6:805–15. [PubMed: 17706564]

[3]. Papadopoulos MC, Verkman AS. Aquaporin water channels in the nervous system. Nat Rev Neurosci. 2013; 14:265–77. [PubMed: 23481483]

[4]. Jarius S, Wildemann B. AQP4 antibodies in neuromyelitis optica: diagnostic and pathogenetic relevance. Nat Rev Neurol. 2010; 6:383–92. [PubMed: 20639914]

[5]. Lennon VA, Kryzer TJ, Pittock SJ, Verkman AS, Hinson SR. IgG marker of optic-spinal multiple sclerosis binds to the aquaporin-4 water channel. J Exp Med. 2005; 202:473–7. [PubMed: 16087714]

[6]. Papadopoulos MC, Verkman AS. Aquaporin 4 and neuromyelitis optica. Lancet Neurol. 2012; 11:535–44. [PubMed: 22608667]

[7]. Ratelade J, Asavapanumas N, Ritchie AM, Wemlinger S, Bennett JL, Verkman AS. Involvement of antibody-dependent cell-mediated cytotoxicity in inflammatory demyelination in a mouse model of neuromyelitis optica. Acta Neuropathol. 2013

[8]. Sabater L, Giralt A, Boronat A, Hankiewicz K, Blanco Y, Llufriu S, et al. Cytotoxic effect of neuromyelitis optica antibody (NMO-IgG) to astrocytes: an in vitro study. J Neuroimmunol. 2009; 215:31–5. [PubMed: 19695715]

[9]. Hengstman GJ, Wesseling P, Frenken CW, Jongen PJ. Neuromyelitis optica with clinical and histopathological involvement of the brain. Mult Scler. 2007; 13:679–82. [PubMed: 17548452]

[10]. Lucchinetti CF, Mandler RN, McGavern D, Bruck W, Gleich G, Ransohoff RM, et al. A role for humoral mechanisms in the pathogenesis of Devic's neuromyelitis optica. Brain. 2002; 125:1450–61. [PubMed: 12076996]

[11]. Misu T, Fujihara K, Kakita A, Konno H, Nakamura M, Watanabe S, et al. Loss of aquaporin 4 in lesions of neuromyelitis optica: distinction from multiple sclerosis. Brain. 2007; 130:1224–34. [PubMed: 17405762]

[12]. Misu T, Hoftberger R, Fujihara K, Wimmer I, Takai Y, Nishiyama S, et al. Presence of six different lesion types suggests diverse mechanisms of tissue injury in neuromyelitis optica. Acta Neuropathol. 2013; 125:815–27. [PubMed: 23579868]

[13]. Roemer SF, Parisi JE, Lennon VA, Benarroch EE, Lassmann H, Bruck W, et al. Pattern-specific loss of aquaporin-4 immunoreactivity distinguishes neuromyelitis optica from multiple sclerosis. Brain. 2007; 130:1194–205. [PubMed: 17282996]

[14]. Zhang H, Bennett JL, Verkman AS. Ex vivo spinal cord slice model of neuromyelitis optica reveals novel immunopathogenic mechanisms. Ann Neurol. 2011; 70:943–54. [PubMed: 22069219]

[15]. Saadoun S, Waters P, Bell BA, Vincent A, Verkman AS, Papadopoulos MC. Intra-cerebral injection of neuromyelitis optica immunoglobulin G and human complement produces neuromyelitis optica lesions in mice. Brain. 2010; 133:349–61. [PubMed: 20047900]

[16]. Saadoun S, Waters P, MacDonald C, Bell BA, Vincent A, Verkman AS, et al. Neutrophil protease inhibition reduces neuromyelitis optica-immunoglobulin G-induced damage in mouse brain. Ann Neurol. 2012; 71:323–33. [PubMed: 22374891]

[17]. Zhang H, Verkman AS. Eosinophil pathogenicity mechanisms and therapeutics in neuromyelitis optica. J Clin Invest. 2013; 123:2306–16. [PubMed: 23563310]

[18]. Pittock SJ, Lennon VA, McKeon A, Mandrekar J, Weinshenker BG, Lucchinetti CF, et al. Eculizumab in AQP4-IgG-positive relapsing neuromyelitis optica spectrum disorders: an open-label pilot study. Lancet Neurol. 2013; 12:554–62. [PubMed: 23623397]

[19]. Zipfel PF, Skerka C. Complement regulators and inhibitory proteins. Nat Rev Immunol. 2009; 9:729–40. [PubMed: 19730437]

[20]. Davies A, Lachmann PJ. Membrane defence against complement lysis: the structure and biological properties of CD59. Immunol Res. 1993; 12:258–75. [PubMed: 7507156]

[21]. Gordon DL, Sadlon T, Hefford C, Adrian D. Expression of CD59, a regulator of the membrane attack complex of complement, on human astrocytes. Brain Res Mol Brain Res. 1993; 18:335–8. [PubMed: 7686996]

[22]. Rogers CA, Gasque P, Piddlesden SJ, Okada N, Holers VM, Morgan BP. Expression and function of membrane regulators of complement on rat astrocytes in culture. Immunology. 1996; 88:153–61. [PubMed: 8707343]

[23]. Spiller OB, Moretto G, Kim SU, Morgan BP, Devine DV. Complement expression on astrocytes and astrocytoma cell lines: failure of complement regulation at the C3 level correlates with very low CD55 expression. J Neuroimmunol. 1996; 71:97–106. [PubMed: 8982108]

[24]. Mead RJ, Neal JW, Griffiths MR, Linington C, Botto M, Lassmann H, et al. Deficiency of the complement regulator CD59a enhances disease severity, demyelination and axonal injury in

murine acute experimental allergic encephalomyelitis. Lab Invest. 2004; 84:21–8. [PubMed: 14631387]

[25]. Miwa T, Zhou L, Hilliard B, Molina H, Song WC. Crry, but not CD59 and DAF, is indispensable for murine erythrocyte protection in vivo from spontaneous complement attack. Blood. 2002; 99:3707–16. [PubMed: 11986227]

[26]. Zhang H, Verkman AS. Aquaporin-4 independent Kir4.1 K+ channel function in brain glial cells. Mol Cell Neurosci. 2008; 37:1–10. [PubMed: 17869537]

[27]. Bennett JL, Lam C, Kalluri SR, Saikali P, Bautista K, Dupree C, et al. Intrathecal pathogenic anti-aquaporin-4 antibodies in early neuromyelitis optica. Ann Neurol. 2009; 66:617–29. [PubMed: 19938104]

[28]. Tradtrantip L, Zhang H, Saadoun S, Phuan PW, Lam C, Papadopoulos MC, et al. Anti-aquaporin-4 monoclonal antibody blocker therapy for neuromyelitis optica. Ann Neurol. 2012; 71:314–22. [PubMed: 22271321]

[29]. Crane JM, Lam C, Rossi A, Gupta T, Bennett JL, Verkman AS. Binding affinity and specificity of neuromyelitis optica autoantibodies to aquaporin-4 M1/M23 isoforms and orthogonal arrays. J Biol Chem. 2011; 286:16516–24. [PubMed: 21454592]

[30]. Hylden JL, Wilcox GL. Intrathecal morphine in mice: a new technique. Eur J Pharmacol. 1980; 67:313–6. [PubMed: 6893963]

[31]. Guyenet SJ, Furrer SA, Damian VM, Baughan TD, La Spada AR, Garden GA. A simple composite phenotype scoring system for evaluating mouse models of cerebellar ataxia. J Vis Exp. 2010; 39:1787. [PubMed: 20495529]

[32]. Laouar Y, Town T, Jeng D, Tran E, Wan Y, Kuchroo VK, et al. TGF-beta signaling in dendritic cells is a prerequisite for the control of autoimmune encephalomyelitis. Proc Natl Acad Sci U S A. 2008; 105:10865–70. [PubMed: 18669656]

[33]. Carter RJ, Lione LA, Humby T, Mangiarini L, Mahal A, Bates GP, et al. Characterization of progressive motor deficits in mice transgenic for the human Huntington's disease mutation. J Neurosci. 1999; 19:3248–57. [PubMed: 10191337]

[34]. Harris CL, Hughes CE, Williams AS, Goodfellow I, Evans DJ, Caterson B, et al. Generation of anti-complement "prodrugs": cleavable reagents for specific delivery of complement regulators to disease sites. J Biol Chem. 2003; 278:36068–76. [PubMed: 12842884]

[35]. Brasoveanu LI, Altomonte M, Fonsatti E, Colizzi F, Coral S, Nicotra MR, et al. Levels of cell membrane CD59 regulate the extent of complement-mediated lysis of human melanoma cells. Lab Invest. 1996; 74:33–42. [PubMed: 8569195]

[36]. Yang LB, Li R, Meri S, Rogers J, Shen Y. Deficiency of complement defense protein CD59 may contribute to neurodegeneration in Alzheimer's disease. J Neurosci. 2000; 20:7505–9. [PubMed: 11027207]

[37]. Yanagawa K, Kawachi I, Toyoshima Y, Yokoseki A, Arakawa M, Hasegawa A, et al. Pathologic and immunologic profiles of a limited form of neuromyelitis optica with myelitis. Neurology. 2009; 73:1628–37. [PubMed: 19917985]

[38]. Baalasubramanian S, Harris CL, Donev RM, Mizuno M, Omidvar N, Song WC, et al. CD59a is the primary regulator of membrane attack complex assembly in the mouse. J Immunol. 2004; 173:3684–92. [PubMed: 15356114]

[39]. Carroll MV, Sim RB. Complement in health and disease. Adv Drug Deliv Rev. 2011; 63:965–75. [PubMed: 21704094]

[40]. Kavanagh D, Richards A, Atkinson J. Complement regulatory genes and hemolytic uremic syndromes. Annu Rev Med. 2008; 59:293–309. [PubMed: 17705684]

[41]. Unsworth DJ. Complement deficiency and disease. J Clin Pathol. 2008; 61:1013–7. [PubMed: 18495794]

[42]. Nevo Y, Ben-Zeev B, Tabib A, Straussberg R, Anikster Y, Shorer Z, et al. CD59 deficiency is associated with chronic hemolysis and childhood relapsing immune-mediated polyneuropathy. Blood. 2013; 121:129–35. [PubMed: 23149847]

[43]. Stahel PF, Flierl MA, Morgan BP, Persigehl I, Stoll C, Conrad C, et al. Absence of the complement regulatory molecule CD59a leads to exacerbated neuropathology after traumatic brain injury in mice. J Neuroinflammation. 2009; 6:2. [PubMed: 19133139]

[44]. Harhausen D, Khojasteh U, Stahel PF, Morgan BP, Nietfeld W, Dirnagl U, et al. Membrane attack complex inhibitor CD59a protects against focal cerebral ischemia in mice. J Neuroinflammation. 2010; 7:15. [PubMed: 20202211]

[45]. Britschgi M, Takeda-Uchimura Y, Rockenstein E, Johns H, Masliah E, Wyss-Coray T. Deficiency of terminal complement pathway inhibitor promotes neuronal tau pathology and degeneration in mice. J Neuroinflammation. 2012; 9:220. [PubMed: 22989354]

[46]. Elvington A, Atkinson C, Zhu H, Yu J, Takahashi K, Stahl GL, et al. The alternative complement pathway propagates inflammation and injury in murine ischemic stroke. J Immunol. 2012; 189:4640–7. [PubMed: 23028050]

[47]. Liu D, Ni B, Wang L, Zhang M, Liu W, Wu Y. Hepatitis B virus core protein interacts with CD59 to promote complement-mediated liver inflammation during chronic hepatitis B virus infection. FEBS Lett. 2013; 587:3314–20. [PubMed: 24036449]

[48]. Giddings KS, Zhao J, Sims PJ, Tweten RK. Human CD59 is a receptor for the cholesterol-dependent cytolysin intermedilysin. Nat Struct Mol Biol. 2004; 11:1173–8. [PubMed: 15543155]

[49]. Yoshimura S, Isobe N, Matsushita T, Yonekawa T, Masaki K, Sato S, et al. Distinct genetic and infectious profiles in Japanese neuromyelitis optica patients according to anti-aquaporin 4 antibody status. J Neurol Neurosurg Psychiatry. 2013; 84:29–34. [PubMed: 23038741]

[50]. Qin X, Goldfine A, Krumrei N, Grubissich L, Acosta J, Chorev M, et al. Glycation inactivation of the complement regulatory protein CD59: a possible role in the pathogenesis of the vascular complications of human diabetes. Diabetes. 2004; 53:2653–61. [PubMed: 15448097]

[51]. Sellner J, Hemmer B, Muhlau M. The clinical spectrum and immunobiology of parainfectious neuromyelitis optica (Devic) syndromes. J Autoimmun. 2010; 34:371–9. [PubMed: 19853412]

[52]. Warabi Y, Yamazaki M, Shimizu T, Nagao M. Abnormal nerve conduction study findings indicating the existence of peripheral neuropathy in multiple sclerosis and neuromyelitis optica. Biomed Res Int. 2013; 2013:847670. [PubMed: 24308009]

[53]. Singhrao SK, Neal JW, Rushmere NK, Morgan BP, Gasque P. Spontaneous classical pathway activation and deficiency of membrane regulators render human neurons susceptible to complement lysis. Am J Pathol. 2000; 157:905–18. [PubMed: 10980130]

[54]. Veerhuis R, Nielsen HM, Tenner AJ. Complement in the brain. Mol Immunol. 2011; 48:1592–603. [PubMed: 21546088]

[55]. Phuan PW, Zhang H, Asavapanumas N, Leviten M, Rosenthal A, Tradtrantip L, et al. C1q-targeted monoclonal antibody prevents complement-dependent cytotoxicity and neuropathology in in vitro and mouse models of neuromyelitis optica. Acta Neuropathol. 2013; 125:829–40. [PubMed: 23677375]

[56]. Spiller OB, Criado-Garcia O, Rodriguez De Cordoba S, Morgan BP. Cytokine-mediated up-regulation of CD55 and CD59 protects human hepatoma cells from complement attack. Clin Exp Immunol. 2000; 121:234–41. [PubMed: 10931136]

[57]. Moutabarrik A, Nakanishi I, Namiki M, Hara T, Matsumoto M, Ishibashi M, et al. Cytokine-mediated regulation of the surface expression of complement regulatory proteins, CD46 (MCP), CD55 (DAF), and CD59 on human vascular endothelial cells. Lymphokine Cytokine Res. 1993; 12:167–72. [PubMed: 7688580]

[58]. Cheng Y, Gao M. The effect of glycation of CD59 on complement-mediated cytolysis. Cell Mol Immunol. 2005; 2:313–7. [PubMed: 16274631]

[59]. Kraus S, Seger R, Fishelson Z. Involvement of the ERK mitogen-activated protein kinase in cell resistance to complement-mediated lysis. Clin Exp Immunol. 2001; 123:366–74. [PubMed: 11298121]

[60]. Gandhi J, Cashman SM, Kumar-Singh R. Soluble CD59 expressed from an adenovirus in vivo is a potent inhibitor of complement deposition on murine liver vascular endothelium. PLoS One. 2011; 6:e21621. [PubMed: 21720565]

[61]. Cashman SM, Ramo K, Kumar-Singh R. A non membrane-targeted human soluble CD59 attenuates choroidal neovascularization in a model of age related macular degeneration. PLoS One. 2011; 6:e19078. [PubMed: 21552568]

[62]. Bora NS, Jha P, Lyzogubov VV, Kaliappan S, Liu J, Tytarenko RG, et al. Recombinant membrane-targeted form of CD59 inhibits the growth of choroidal neovascular complex in mice. J Biol Chem. 2010; 285:33826–33. [PubMed: 20736175]

[63]. Fraser DA, Harris CL, Williams AS, Mizuno M, Gallagher S, Smith RA, et al. Generation of a recombinant, membrane-targeted form of the complement regulator CD59: activity in vitro and in vivo. J Biol Chem. 2003; 278:48921–7. [PubMed: 14519760]

[64]. LoPachin RM, Rudy TA. Sites and mechanism of action for the effects of intrathecal noradrenaline on thermoregulation in the rat. J Physiol. 1983; 341:527–44. [PubMed: 6688637]

[65]. Kinoshita M, Nakatsuji Y, Kimura T, Moriya M, Takata K, Okuno T, et al. Neuromyelitis optica: Passive transfer to rats by human immunoglobulin. Biochem Biophys Res Commun. 2009; 386:623–7. [PubMed: 19545538]

[66]. Asgari N, Khorooshi R, Lillevang ST, Owens T. Complement-dependent pathogenicity of brain-specific antibodies in cerebrospinal fluid. J Neuroimmunol. 2013; 254:76–82. [PubMed: 23031833]

Highlights

- CD59 is an important modulator of the immune response in NMO.
- CD59 inactivation greatly increases NMO-IgG cytotoxicity and NMO pathology in mice.
- A single intrathecal injection of NMO-IgG in CD59 null mice produced longitudinally extensive spinal cord pathology, as seen in human NMO.
- Upregulation of CD59 expression may be a new therapeutic option in NMO

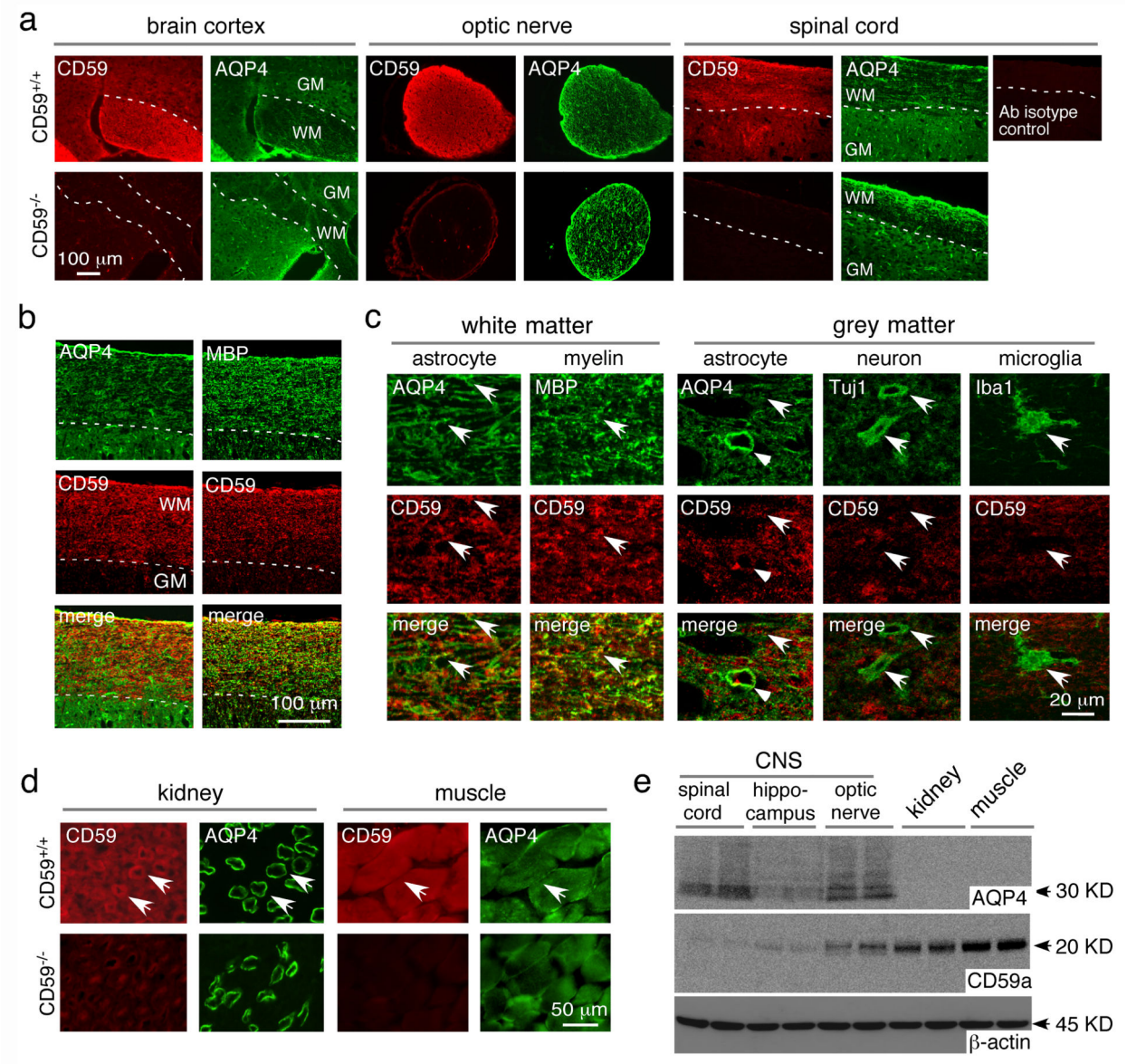

Fig. 1. CD59 expression in mice

a. CD59 and AQP4 immunofluorescence in brain cortex, optic nerve and spinal cord of $CD59^{+/+}$ and $CD59^{-/-}$ mice. GM grey matter, WM white matter. CD59 antibody isotype control shown on the right. **b.** AQP4, MBP and CD59 immunofluorescence in spinal cord white matter. **c**. High magnification of spinal cord white matter and grey matter showing CD59 immunostaining with different cell markers - AQP4, MBP, Tuj1 and Iba1. Arrows indicates co-expression, arrowheads astrocyte end-feet, V vessel. **d.** CD59 and AQP4 immunofluorescence in kidney and skeletal muscle of $CD59^{+/+}$ and $CD59^{-/-}$ mice. **e.** CD59, AQP4 and β-actin immunoblot of brain and peripheral tissue homogenates.

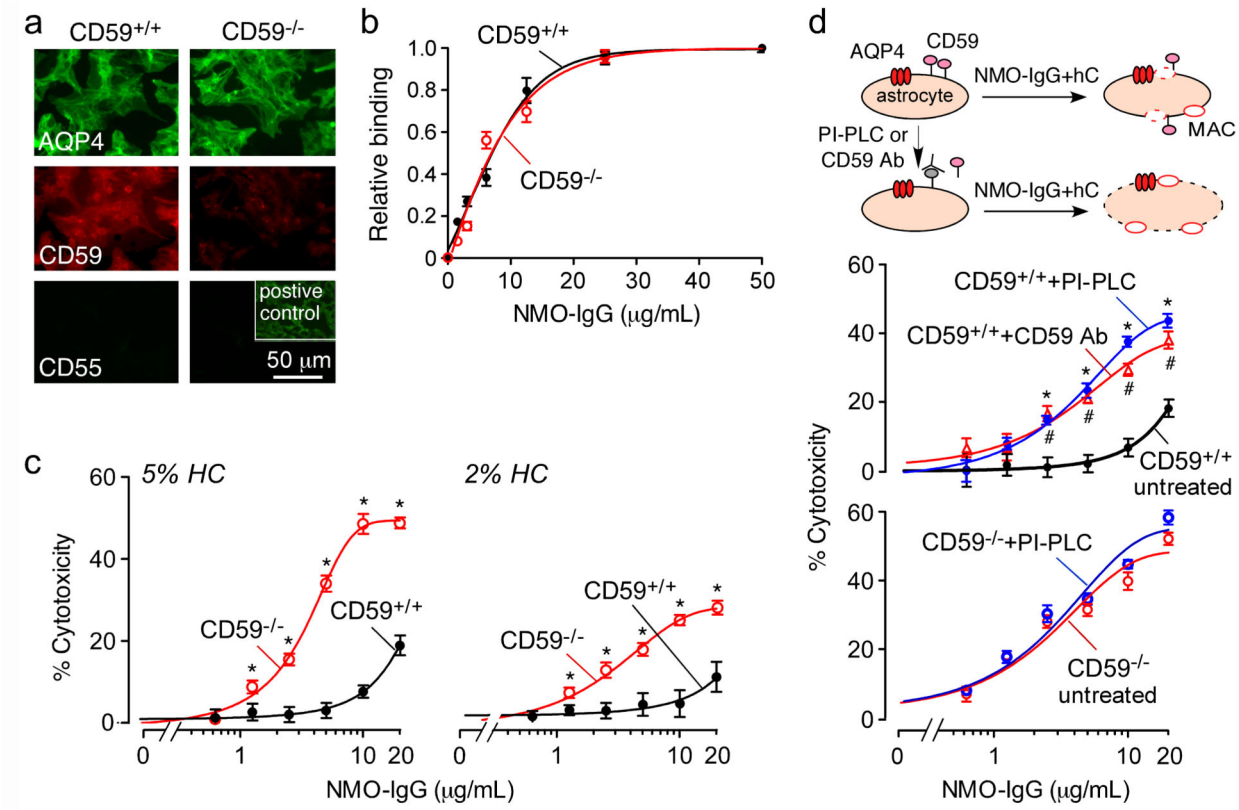

Fig. 2. CD59 neutralization or deletion protects against NMO-IgG- and complement-dependent cytotoxicity in astrocyte cultures

a. AQP4, CD59 and CD55 immunofluorescence in primary astrocyte cultures from $CD59^{+/+}$ and $CD59^{-/-}$ mice. Insert shows CD55 staining of mouse lung as positive control. **b.** NMO-IgG binding to astrocyte cultures shown as normalized ratio of NMO-IgG to AQP4 fluorescence ('relative binding'), as a function of NMO-IgG concentration (S.E., n=6). Differences not significant. **c.** CDC (by Alamar blue assay) in cultures incubated with 5% (left) or 2% (right) human complement and NMO-IgG (0-20 μg/ml) (S.E., n=6, * $P < 0.05$, comparing with $CD59^{+/+}$ astrocytes). **d.** (top) Experimental protocol. MAC, membrane attack complex. (middle) CDC in $CD59^{+/+}$ astrocyte cultures without and after treatment mCD59a neutralizing Ab (CD59 Ab, 10 μg/mL, S.E., n=6, # $P < 0.05$, comparing with the untreated group) or PI-PLC (0.5 U/mL) (S.E., n=6, * $P < 0.05$, comparing with the untreated group). (bottom) CDC in control and PI-PLC-treated $CD59^{-/-}$ astrocyte cultures (S.E., n=6).

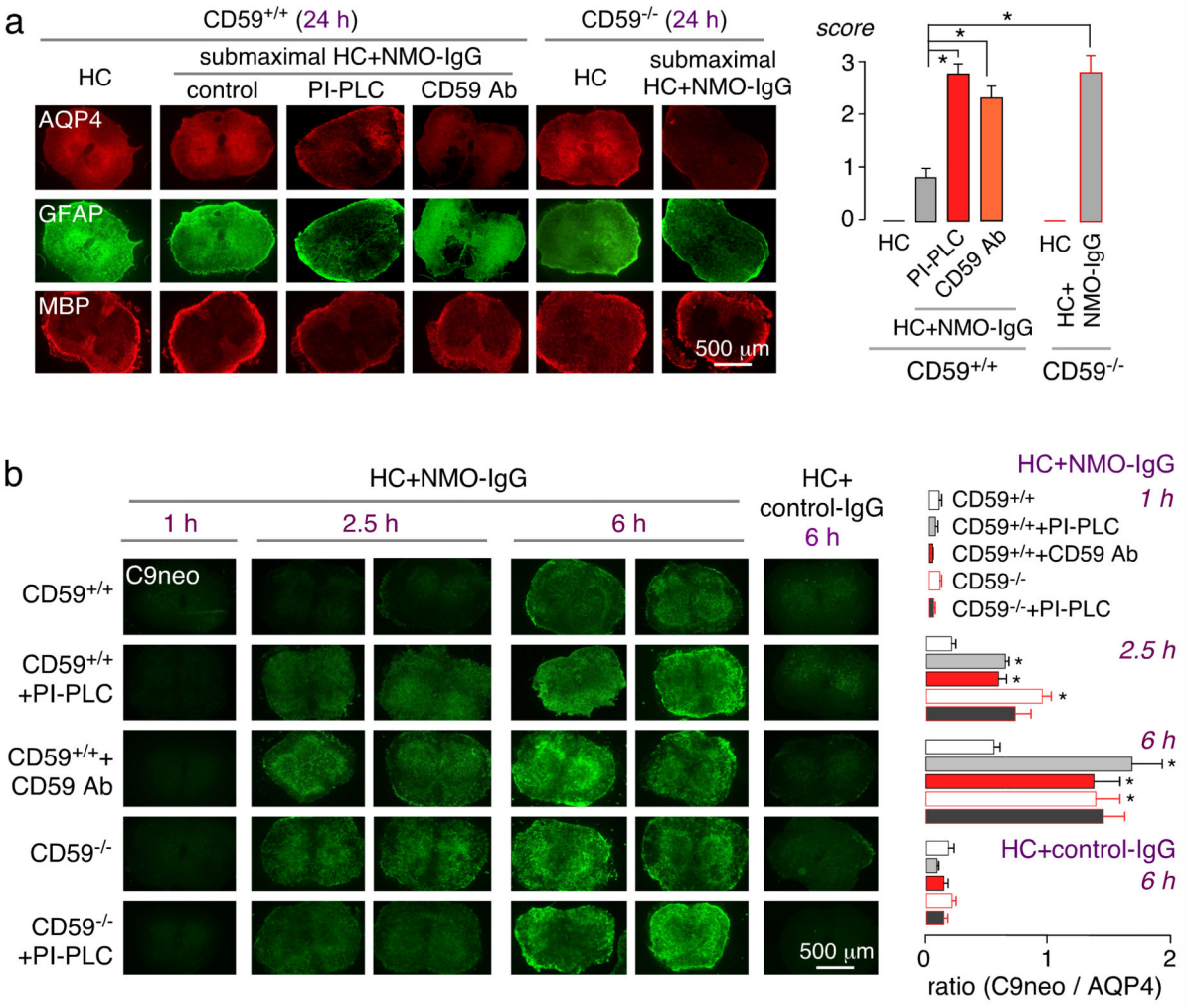

Fig. 3. CD59 neutralization or deletion protects against NMO-IgG-dependent CDC and demyelination in *ex vivo* spinal cord slice cultures

a. Vibratome-cut spinal cord slices from CD59$^{+/+}$ and CD59$^{-/-}$ mice were cultured on a porous support for 7 days, followed by addition of NMO-IgG (5 μg/mL) and submaximal human complement (5%), CD59 Ab (10 μg/mL) or PI-PLC (0.5 U/mL). (left) AQP4, GFAP and MBP immunofluorescence of spinal cord slices. (right) Summary of pathology scores (S.E., 5 slices per condition, * P < 0.001). **b.** (left) C5b-9 immunofluorescence after 1, 2.5 and 6 h incubation with human complement (5 %) and NMO-IgG (10 μg/mL), with or without CD59 Ab (10 μg/mL) or PI-PLC (0.5 U/mL). (right) C9neo / AQP4 immunofluorescence ratios (S.E., 6 slices per condition, * P < 0.01).

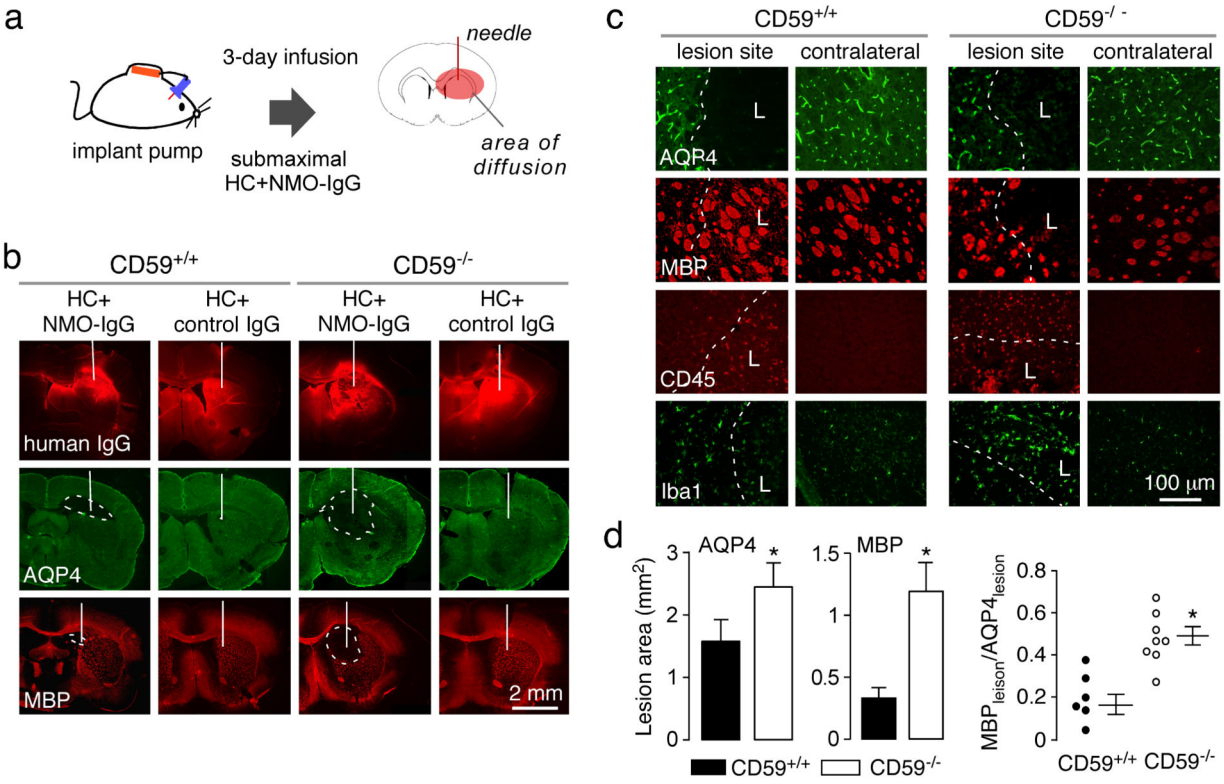

Fig. 4. Greatly increased NMO pathology in CD59$^{-/-}$ mice following intracerebral infusion of NMO-IgG and human complement

a. Diagram of the mini-pump infusion model. **b.** NMO-IgG ('human IgG' using anti-human secondary antibody), AQP4 and MBP immunofluorescence at 3 days after continuous infusion of NMO-IgG and complement in CD59$^{+/+}$ and CD59$^{-/-}$ mice. White line indicates the needle track and dashed line the lesion area (representative of 6 mice per group). **c.** Higher magnification showing AQP4, MBP, CD45 and Iba1 immunofluorescence in the lesion and in contralateral brain. Dashed line indicates the boundary of AQP4 loss. L: lesion area. **d.** Summary of areas of AQP4 and MBP loss, and relative MBP vs. AQP4 loss (S.E., n=6, * $P < 0.05$).

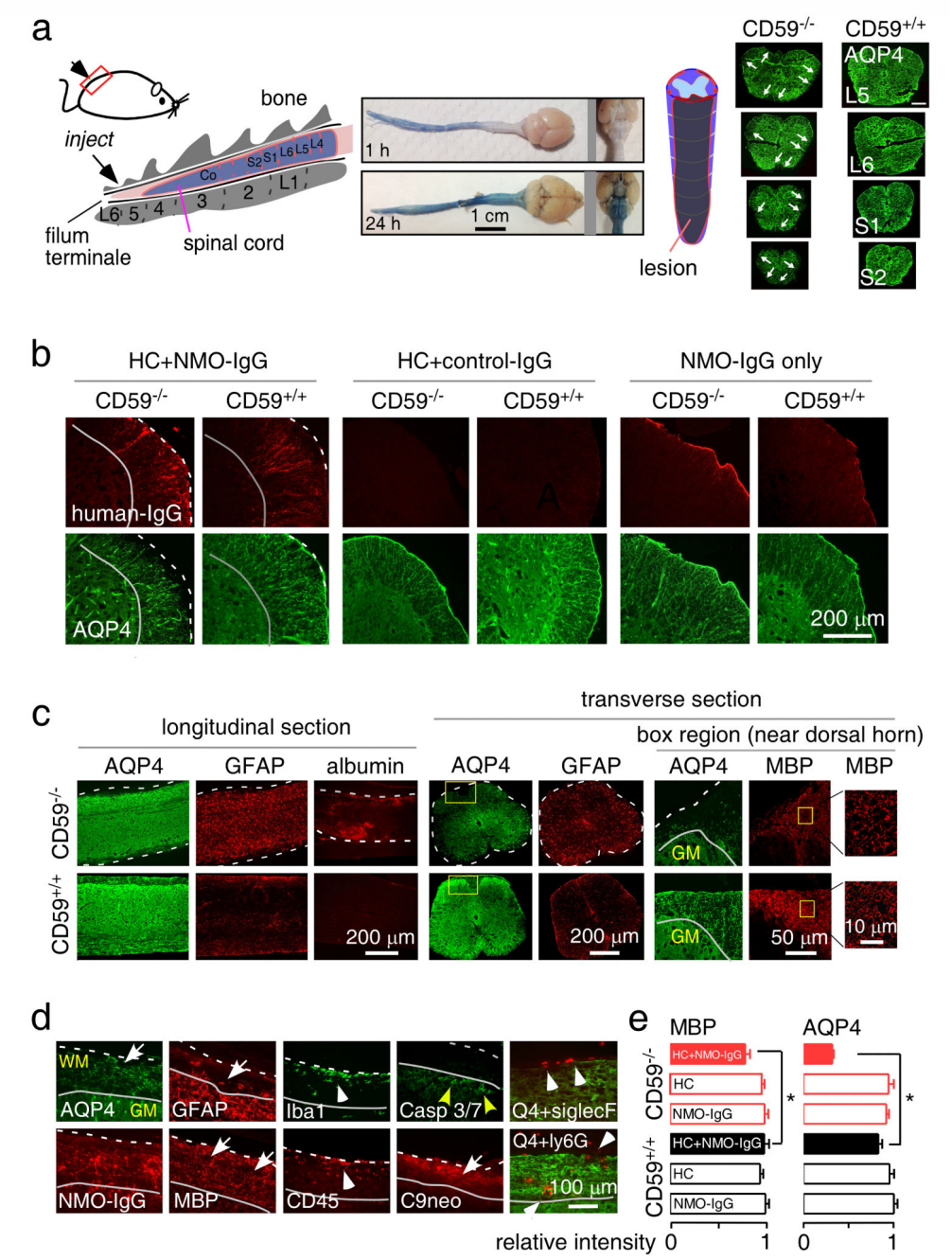

Fig. 5. Longitudinally extensive white-matter lesions in CD59$^{-/-}$ mice after intrathecal injection of NMO-IgG and human complement

a. (left) Diagram of the intrathecal injection model: 10 µg of recombinant NMO-IgG (or control IgG) and 5 µL human complement in total volume of 10 µL was injected. (middle) Evan's blue dye diffusion at 1 and 24 h after intrathecal injection at L6 (representative of 5 mice per time point). (right) Diagram of spinal cord showing lesion volume along with transverse sections (arrows indicate lesion). Scale bar: 200 µm. Representative of 3 mice per group. **b.** Human IgG and AQP4 immunofluorescence in transverse spinal cord sections of CD59$^{+/+}$ and CD59$^{-/-}$ mice treated as indicated. Dashed line indicates the edge of white

matter, solid line the interface between white and grey matter, and arrow the lesion. **c.** AQP4, GFAP, and albumin immunofluorescence in longitudinal (left) and transverse (right) spinal cord sections in $CD59^{+/+}$ and $CD59^{-/-}$ mice at 2 days after receiving NMO-IgG and human complement. Dashed line indicates the edge of white matter and arrow the lesion. High magnification of boxed regions shown at the right. Representative of 5 mice per group. **d**. High magnification showing AQP4, GFAP, MBP, C9neo, human IgG, cleaved caspase3/7 (apoptotic cell marker), Siglec-F (eosinophil marker), Ly6G (neutrophil marker) and Iba1 (macrophage/microglia marker) immunofluorescence. WM: white matter. Dashed line indicates the edge of white matter, solid line interface between white and grey matter, white arrow the lesion, white arrowhead infiltrating cells, and yellow arrow apoptotic motor neurons. **e**. AQP4 and MBP immunofluorescence in L5 spinal cord sections, showing relative intensity normalized to control $CD59^{+/+}$ or $CD59^{-/-}$ sections. For each mouse, 3 different sections were averaged (S.E., n=5-6 mice, * $P < 0.05$).

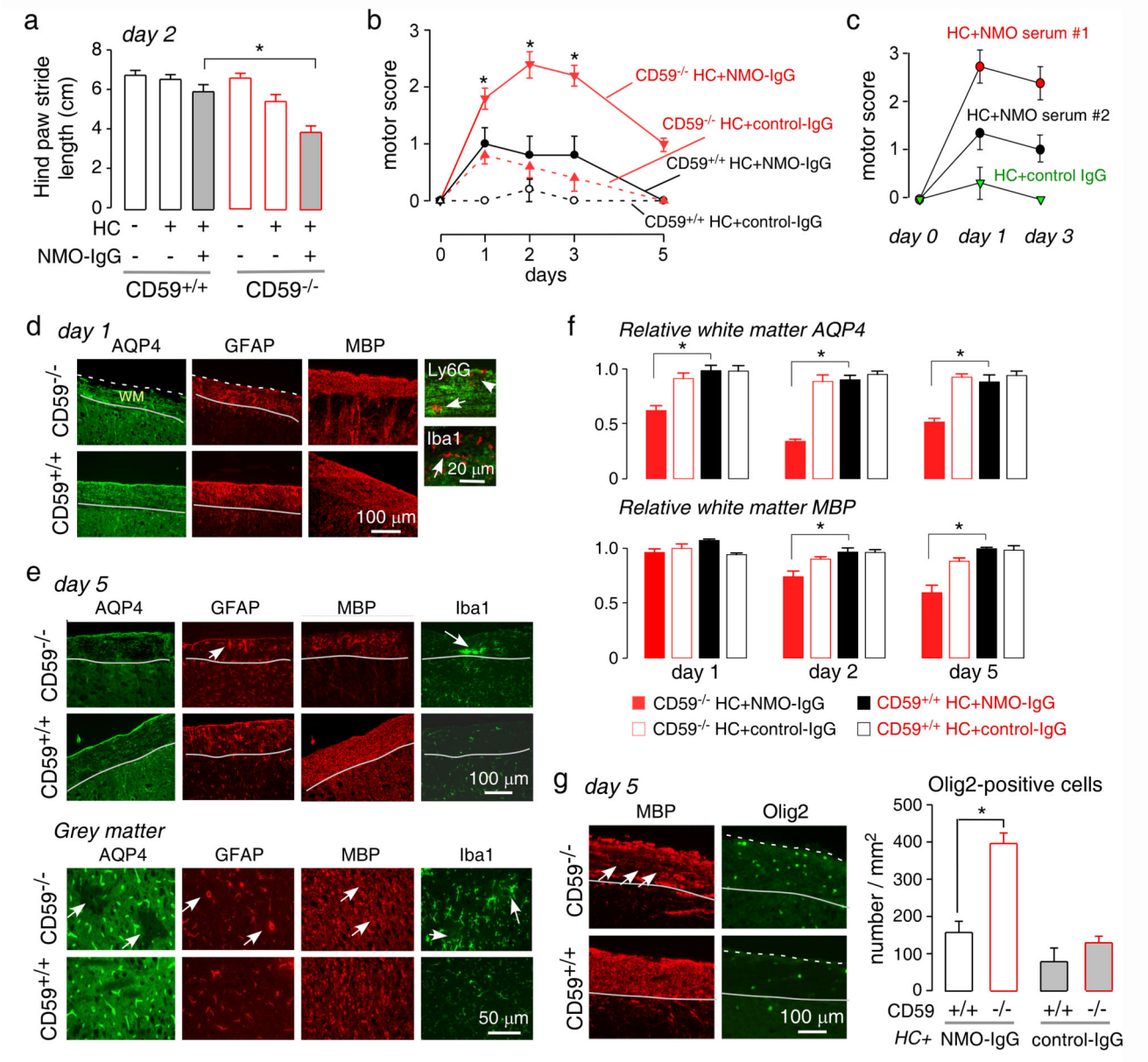

Fig. 6. Progression of NMO pathology in CD59$^{-/-}$ mice following intrathecal injection of NMOIgG

a. Hind paw stride length at day 2 (S.E., 6-8 mice per group, * P < 0.01). **b.** Motor scores in CD59$^{+/+}$ and CD59$^{-/-}$ mice, treated with control or NMO-IgG and human complement (S.E., 6-8 mice per group, * P < 0.01). **c.** Motor scores in CD59$^{-/-}$ mice receiving two NMO sera (or control serum) and human complement at 3 days (S.E., n=4, * P < 0.01). **d.** AQP4, GFAP, MBP, Iba1 and Ly6G immunofluorescence at 1 day after intrathecal injection (representative of 5 mice). Dashed line indicates the edge of white matter, solid line the interface between white and grey matter, white arrowhead infiltrating cells. **e.** AQP4, GFAP, MBP and Iba1 immunofluorescence in white and grey matter at 5 days after intrathecal injection. Solid line indicates interface between white and grey matter, yellow arrow reactive astrocytes, white arrowhead aggregated microglia/macrophage, white arrow the

lesion (representative of 5 mice per group). **f.** AQP4 and MBP immunofluorence in L5 spinal cord sections at different days after intrathecal injection, showing relative intensity normalized to control $CD59^{+/+}$ or $CD59^{-/-}$ sections. For each mouse, 3 different sections were averaged (S.E., n=5-6 mice, * $P < 0.05$). **g.** (left) Olig2 and MBP immunofluorescence in white matter at day 5. White arrow indicates the lesion. (right) Olig2-positive cells in each group (S.E., 5 mice studied with 5 contiguous sections analyzed per mouse, * $P < 0.01$).

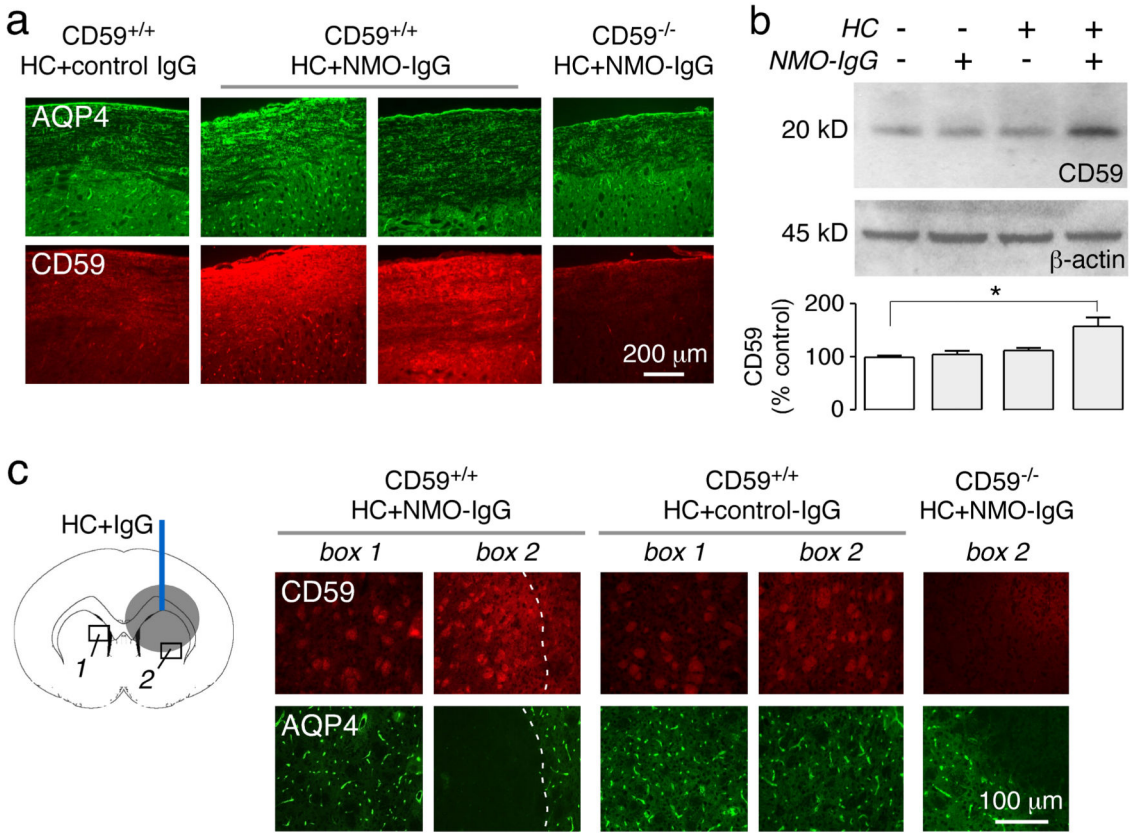

Fig. 7. CD59 up-regulation in CD59$^{+/+}$ mice following induction of NMO pathology

a. (left) Expression of CD59 and AQP4 at the L4 level at 2 days after intrathecal injection of control or NMOIgG and human complement, showing micrographs from two mice. CD59$^{-/-}$ mouse shown as control (representative of 5 mice per group). **b.** CD59 and β-actin immunoblot of spinal cord homogenates of three CD59$^{+/+}$ mice. Data representative of 3 sets of experiments (S.E. n=3, * $P < 0.05$). **c.** (left) Diagram of brain infusion model. (right) CD59 and AQP4 immunofluorescence in boxed regions. Dashed line indicates the edge of AQP4 loss, L lesion area (representative of 5 mice per group).